Available on the CERN CDS information server **CMS PAS FTR-18-037**

CMS Physics Analysis Summary

Contact: cms-phys-conveners-ftr@cern.ch 2019/02/14

HL-LHC searches for new physics in hadronic final states with boosted W bosons or top quarks using razor variables

The CMS Collaboration

Abstract

We present High-Luminosity LHC (HL-LHC) projections of the Run 2 search for new physics in hadronic final states with boosted W bosons or top quarks using razor variables. Data event yields and signal/background cross sections from the 2016 analysis are scaled to obtain the HL-LHC sensitivity for center-of-mass energy of 14 TeV and integrated luminosity of 3 ab^{-1}. Different scenarios for systematic uncertainties are considered. The projection results are interpreted in terms of gluino pair production where each gluino decays to a top quark, an anti-top quark, and a neutralino; or to a top quark and a top squark; and direct top squark pair production where each top squark decays to a top quark and a neutralino.

1 Introduction

This note presents the projection of the CMS search for new physics with boosted W bosons or top quarks using the razor kinematic variables to the High-Luminosity LHC (HL-LHC) conditions of center-of-mass energy of 14 TeV and integrated luminosity of 3 ab^{-1}. The projected search performed on the Run 2 2016 dataset is part of a larger inclusive new physics search with razor variables that includes an extensive set of hadronic and leptonic search regions, documented in [1].

The analysis targets final states consistent with supersymmetry (SUSY), and in particular, with a realization of it called natural SUSY [2, 3]. This specific scenario requires the existence of a light top squark, $\widetilde{t}_1$, and a somewhat light gluino, $\widetilde{g}$, which stabilize the Higgs field mass-squared term without excessive fine tuning. Observing light gluinos and top squarks at the LHC would provide a test for naturalness. The possibility that the top squark could be light has motivated several searches by the CMS and ATLAS collaborations for the direct production of top squarks. However, these searches tend to lose sensitivity in a few particular scenarios. One such scenario, called the compressed scenario, occurs when the mass of the $\widetilde{t}_1$ approaches that of the lightest SUSY particle (LSP), assumed to be the lightest neutralino, $\widetilde{\chi}_1^0$. A second scenario, called the diagonal scenario, occurs when the mass difference between the top squark and the LSP is around the top quark mass, $\Delta m = m_{\widetilde{t}_1} - m_{\widetilde{\chi}_1^0} \approx m_t$. The diagonal scenario reduces the sensitivity of searches looking specifically for $\widetilde{t}_1 \to t\widetilde{\chi}_1^0$.

In the compressed scenario, the $\widetilde{t}_1$ decays either through a 4-body decay to $bf\bar{f}\widetilde{\chi}_1^0$, where f is any fermion, or through the loop-induced decay to $c\widetilde{\chi}_1^0$. In both scenarios, the decay products of the top squark generally have very low transverse momentum (p_T) and therefore are very hard to detect. In order to be sensitive to such cases, it is necessary to rely on another property of the events, often the presence of initial state radiation (ISR) jets. Instead, the search can target top squarks produced in a slightly longer decay chain. One possible assumption is that the heavy top squark $\widetilde{t}_2$ is also accessible and decays to the $\widetilde{t}_1$ via a Higgs or Z boson. Alternatively, one may postulate the existence of a gluino and search for top squarks from gluino decays.

This analysis targets gluino production, where the gluino decays to a top squark and a top quark. The Run 2 analysis excluded scenarios with a gluino mass around 2 TeV and a top squark mass of several hundred GeV; these limits are expected to increase significantly for the HL-LHC. Due to the significant mass gap between the gluino and the top squark, the top quark from the gluino decay receives a large boost. The top squark then decays, as in one of the scenarios explained above, to $c\widetilde{\chi}_1^0$ for small Δm. The simplified model [4, 5] corresponding to this topology is called T5ttcc. In addition to these models, we also consider gluinos directly decaying to $t\bar{t}\widetilde{\chi}_1^0$, called T1tttt, and direct production of top squark pairs, where each top squark decays to a top quark and a neutralino, called T2tt. All of these models are illustrated by the diagrams in Fig. 1.

Boosted objects, which have high p_T, are characterized by merged decay products separated by $\Delta R \sim 2m/p_T$, where m denotes the mass of the decaying massive particle. A top quark or W boson can be identified via boosted objects within a jet of size 0.8 if it has a momentum of $\gtrsim$430 GeV or $\gtrsim$200 GeV, respectively. As boosted objects become more accessible at the increased center-of-mass energies, they will be produced more frequently at the HL-LHC. Therefore this analysis is an interesting addition to the HL-LHC studies.

Figure 2 shows the generator-level p_T distributions for W bosons and top quarks from the gluino decay for several mass points of the T5ttcc simplified models, compared to the W boson and top quark p_T distributions from the standard model (SM) $t\bar{t}$+jets process. An initial

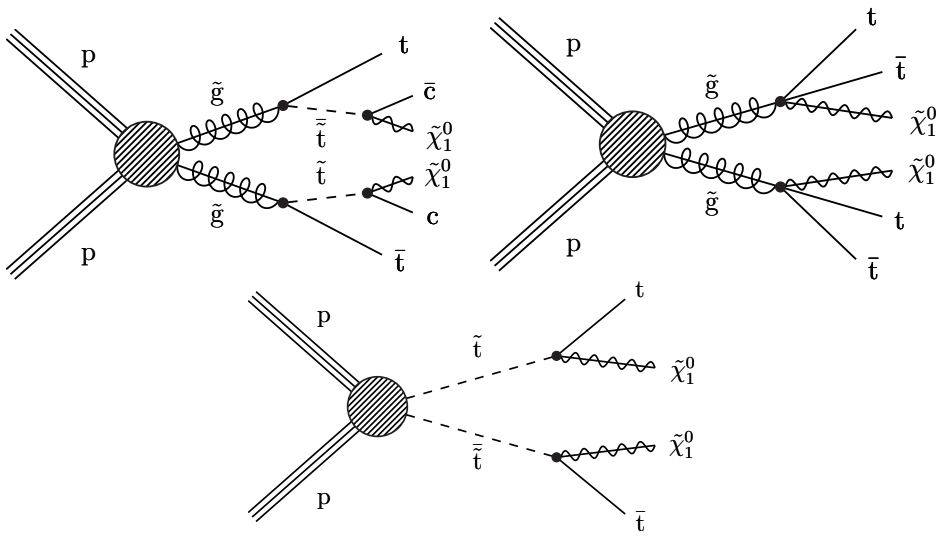

Figure 1: Signal models considered in this analysis: T5ttcc (top left), T1tttt (top right), and T2tt (bottom).

selection of a jet having size 0.8 with $p_T > 200\,\text{GeV}$ and razor variable $R^2 > 0.04$ has been applied to events shown in Fig. 2. From these distributions we can see that the W bosons and top quarks in the signal models have significantly higher momenta compared to the SM $t\bar{t}$+jets process. This shows that the boosted top quarks and W bosons are a promising signature in new physics searches.

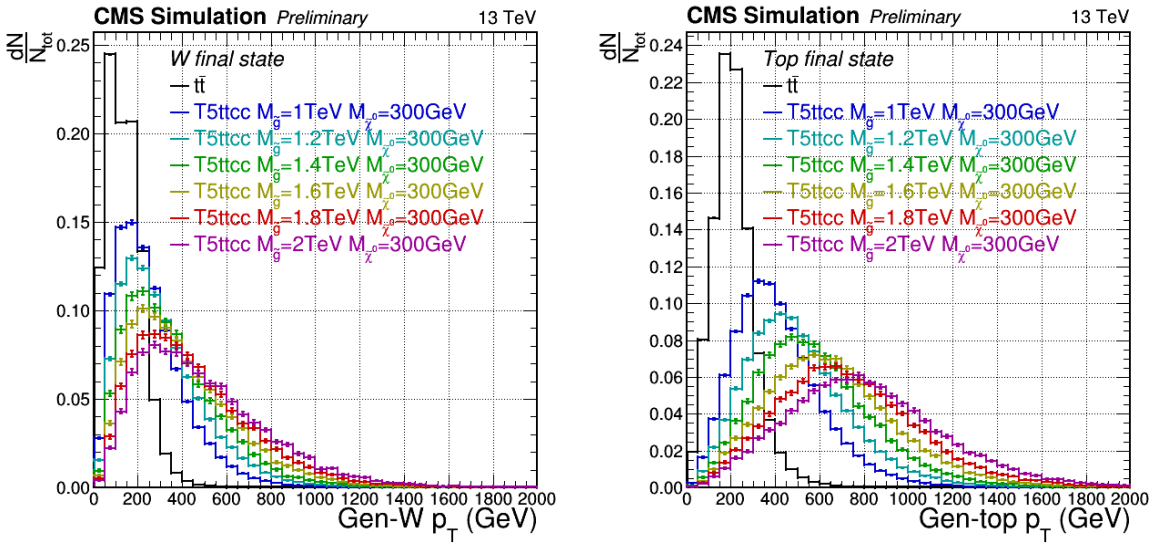

Figure 2: Generator-level W boson and top quark p_T distributions for several signal points from the T5ttcc simplified model, compared to the $t\bar{t}$+jets background. Only a set of events selected with a requirement of a jet with size 0.8, $p_T > 200\,\text{GeV}$, and razor variable $R^2 > 0.04$, as explained in the text, are shown.

The analysis is performed in hadronic topologies with boosted top quarks, or boosted W bosons and b jets, using the razor kinematic variables (to be defined in Section 2), which are powerful tools that help to discriminate between SM processes and production of heavy new particles decaying to final states with massive invisible particles and massless visible particles. The analysis is performed in three signal search regions defined by selections on the razor variables. Boosted top quarks and W bosons are identified by finding massive jets that possess

substructure, which can be identified with the n-subjettiness technique [6].

In this note, we will first introduce the razor variables in Section 2, followed by the HL-LHC and the upgraded CMS detector in Section 3. We will then explain the analysis methodology in Section 4, followed by the details of the projection of MC and data events in Section 5 and treatment of uncertainties in Section 6. Finally, we will present our results and their interpretation in Section 7, followed by the summary in Section 8.

2 The razor variables

The razor variables M_R and R^2 map the event into a dijet topology [7]. They help to describe a signal coming from pair production of two heavy particles, each decaying to a massless visible particle and a massive invisible particle, as a peak over exponentially falling SM backgrounds. For this reason, the razor variables are robust discriminators for SUSY signals with pair-produced sparticles that subsequently decay to lighter SM particles and the invisible LSPs. For the simple case where the final topology has two visible particles, e.g., jets j_1 and j_2, the razor variables are defined using the 4-momenta of these two jets $(E^{j_i}, \vec{p}_{\mathrm{T}}^{\,j_i}, p_z^{j_i})$, where $i = 1, 2$, and the missing transverse momentum $\vec{p}_{\mathrm{T}}^{\,\mathrm{miss}}$, with magnitude $p_{\mathrm{T}}^{\mathrm{miss}}$, as

$$M_R \equiv \sqrt{\left(E^{j_1} + E^{j_2}\right)^2 - \left(p_z^{j_1} + p_z^{j_2}\right)^2} \tag{1}$$

$$M_{\mathrm{T}}^R \equiv \sqrt{\frac{p_{\mathrm{T}}^{\mathrm{miss}}\left(p_{\mathrm{T}}^{j_1} + p_{\mathrm{T}}^{j_2}\right) - \vec{p}_{\mathrm{T}}^{\,\mathrm{miss}} \cdot \left(\vec{p}_{\mathrm{T}}^{\,j_1} + \vec{p}_{\mathrm{T}}^{\,j_2}\right)}{2}}. \tag{2}$$

Given M_R and M_{T}^R, the razor dimensionless ratio is defined as

$$R \equiv \frac{M_{\mathrm{T}}^R}{M_R}. \tag{3}$$

However, if the decay chains are more complicated and there are multiple particles in the final state, we first form two "megajets" from the final state particles, such that each of the megajets contain the particles coming from one of the heavy pair-produced particles. M_R and R^2 are then computed using the 4-momenta of these two megajets, where the megajet 4-momenta are computed as the vectorial sums of the 4-momenta of the jets contributing to each megajet. Of all the possible partitions of the jets into two megajets, we select the combination that minimizes the sum of the invariant masses of the two megajets. This choice will cluster together particles that are traveling in the same direction, and it has been found to perform well.

3 Upgraded CMS detector

The CMS detector [8] will be substantially upgraded in order to fully exploit the physics potential offered by the increase in luminosity, and to cope with the demanding operational conditions at the HL-LHC [9–13]. The upgrade of the first level hardware trigger (L1) will allow for an increase of the L1 rate and latency to about 750 kHz and 12.5 μs, respectively, and the high-level software trigger is expected to reduce the rate by about a factor of 100 to 7.5 kHz. The entire pixel and strip tracker detectors will be replaced to increase the granularity, reduce the material budget in the tracking volume, improve the radiation hardness, and extend the geometrical coverage and provide efficient tracking up to pseudorapidities of about $|\eta| = 4$. The muon system will be enhanced by upgrading the electronics of the existing cathode strip

chambers, resistive plate chambers (RPC) and drift tubes . New muon detectors based on improved RPC and gas electron multiplier technologies will be installed to add redundancy, increase the geometrical coverage up to about $|\eta| = 2.8$, and improve the trigger and reconstruction performance in the forward region. The barrel electromagnetic calorimeter will feature the upgraded front-end electronics that will be able to exploit the information from single crystals at the L1 trigger level, to accommodate trigger latency and bandwidth requirements, and to provide 160 MHz sampling allowing high precision timing capability for photons. The hadronic calorimeter, consisting in the barrel region of brass absorber plates and plastic scintillator layers, will be read out by silicon photomultipliers. The endcap electromagnetic and hadron calorimeters will be replaced with a new combined sampling calorimeter that will provide highly-segmented spatial information in both the transverse and longitudinal directions, as well as high-precision timing information. Finally, the addition of a new timing detector for minimum ionizing particles in both the barrel and endcap regions is envisaged to provide the capability for 4-dimensional reconstruction of interaction vertices that will significantly offset the CMS performance degradation due to high pileup (PU) rates.

A detailed overview of the CMS detector upgrade program is presented in Refs. [9–13], while the expected performance of the reconstruction algorithms and pile-up mitigation with the CMS detector is summarised in Ref. [14].

4 Analysis methodology

The analysis is designed to look for an excess in events with high values of M_R and R^2 in fully hadronic final states with at least one boosted W boson and a b jet, or one boosted top jet.

The 2016 analysis was performed using 35.9 fb^{-1} of 13 TeV proton-proton collision data collected in 2016 [1]. The projection study presented here uses the same data and Monte Carlo (MC) events as in the 2016 analysis. It also follows exactly the same object selection, event selection, background estimation, systematic uncertainty calculation, and limit setting procedures as used in the 2016 analysis. As this is a projection study, event kinematics for individual processes are unchanged. The main differences introduced in the projection study are the scaling of event yields to higher cross sections and luminosities, which will be explained in Section 5, and the scaling of systematic uncertainties to the HL-LHC conditions [14], which will be detailed in Section 6. In the remainder of this section, we outline event selection and background estimation procedures which are directly adapted from the 2016 analysis by the HL-LHC projection study.

The 2016 analysis used data collected by triggers selecting events based on the p_{T} of the leading jet and the scalar sum of the transverse momenta of all jets, H_{T}. These jets are reconstructed using the anti-k_{T} algorithm [15, 16] with distance parameters of $R = 0.8$ (AK8) and $R = 0.4$ (AK4) for the p_{T}-based and H_{T}-based triggers, respectively. As these triggers were only $\approx$70% efficient for the M_R-R^2 selection, efficiencies were modeled as a function of jet p_{T} and H_{T} using orthogonal datasets. This trigger efficiency modeling is also applied in the projection, since data distributions are used in the control regions for background estimation. Detailed description of the objects used in the analysis are given in Ref. [1]. Boosted W bosons and top quarks are identified using the jet mass, the n-subjettiness variables $\tau_{2/1}$ and $\tau_{3/2}$ [6], and subjet b tagging.

Events in all signal, control, and validation regions in the analysis are required to have

- at least one good primary vertex

- at least four selected AK4 jets
- at least one AK8 jet with $p_T > 200\,\text{GeV}$ defining the boosted phase space; and
- $M_R > 800\,\text{GeV}$ and $R^2 > 0.08$, where the megajets are constructed from the selected AK4 jets. This selection, based on the kinematic properties of the target signals, provides an optimal balance between background suppression and signal acceptance.

The signal regions are required to have in addition:

- No leptons fulfilling the veto identification criteria
- Azimuthal distance between the two megajets, $\Delta\phi_{\text{megajets}} < 2.8$
- 3 categories based on boosted object and jet multiplicities are defined:
  - W boson categories: $\geq$1 AK4 b jet (identified with the medium tagger of the combined secondary vertex algorithm [17]) and $\geq$1 reconstructed AK8 W jet. Two bins of AK4 jet multiplicity:
    - W 4-5 jet: $4 \leq n_{\text{jet}} \leq 5$
    - W 6 jet: $n_{\text{jet}} \geq 6$
  - Top quark category (Top): $\geq$1 reconstructed AK8 top jet

The dominant SM backgrounds remaining in the signal regions originate from $\text{t}\bar{\text{t}}$+jets, single top quark production, quantum chromodynamics (QCD) multijet events that have jets produced through the strong interaction, and the $\text{W}(\ell\nu)$+jets and $\text{Z}(\nu\bar{\nu})$+jets processes. Because there are large uncertainties in the simulation modeling for these processes, data-driven methods are employed to estimate their contributions to the signal regions. The estimation method outlined below is directly taken from the 2016 analysis, and its complete details can be found in [1]. The procedure involves control regions that isolate a particular process to be estimated, or a process that can approximately mimic it. These control regions are generally defined by reversing or otherwise modifying one or more signal selection criteria, and are designed to be as similar as possible in kinematic properties to the signal regions, in order to reduce shape uncertainties. The projection study uses the control region definitions from the 2016 analysis as listed below:

- A multijet control region for the QCD multijet estimation obtained by inverting the $\Delta\phi_{\text{megajets}}$ selection, and by reversing the n-subjettiness criterion in the W and top tagging algorithms.
- A $\text{t}\bar{\text{t}}$+jets and single top control region for the $\text{t}\bar{\text{t}}$+jets and single top estimation, which requires exactly 1 lepton (ℓ = e or μ), and transverse mass $m_T = \sqrt{2p_T^{\ell} p_T^{\text{miss}}(1 - \cos\Delta\phi(\vec{p}_T^{\,\ell}, \vec{p}_T^{\,\text{miss}}))} < 100\,\text{GeV}$.
- A W+jets control region for the W+jets estimation, which requires exactly 1 lepton, 0 b jets, reversed subjet b tagging in the top tagging algorithm, and $30 < m_T < 100\,\text{GeV}$.
- A γ+jets control region for the $\text{Z}(\nu\bar{\nu})$+jets estimation, with exactly 1 photon whose $\vec{p}_T$ is added to the $\vec{p}_T^{\,\text{miss}}$, 1 W- or top-tagged jet with only the jet mass requirement applied, and no requirement on b jets.
- A $\text{Z}(\ell^+\ell^-)$+jets control region with 2 same-flavor leptons (ee or $\mu\mu$) whose $\vec{p}_T$ are added to the $\vec{p}_T^{\,\text{miss}}$, 1 W- or top-tagged jet with only the jet mass requirement applied, and no requirement on b jets. This control region is used for correcting the primary $\text{Z}(\nu\bar{\nu})$+jets estimate, which uses the γ+jets control region defined above.
- A $\text{W}(\ell\nu)$+jets control region with exactly 1 lepton (e or μ) whose $\vec{p}_T$ is added to the $\vec{p}_T^{\,\text{miss}}$, $30 < m_T < 100\,\text{GeV}$, 1 W- or top-tagged jet with only the jet mass requirement

applied, and no requirement on b jets. This control region is used to cross-check the $Z(\nu\overline{\nu})$+jets estimate and to derive a systematic uncertainty based on the difference with respect to the primary estimate from the γ+jets control region.

Data and simulation event yields in these regions are scaled to the HL-LHC cross sections, as described in Section 5. After scaling all distributions, background estimates in the signal regions are obtained by multiplying the observed data yields, binned in M_R and R^2, by the simulation transfer factors computed as the ratios of the yields of background MC simulation events in the signal regions to the yields in control regions. Other SM processes that contribute less significantly, such as VV, VVV, and $t\bar{t}V$, are estimated directly from the simulation, scaled to the HL-LHC cross sections and luminosities. The simulated events used for obtaining both the transfer factors and the direct estimates are corrected using various data-to-simulation correction factors and event weights. The uncertainties in these correction factors and weights are taken into account as systematic uncertainties (see Section 6). The validity of this background estimation procedure was established in the 2016 analysis by closure tests in two validation regions that resemble the topology and kinematic properties of the signal regions, but are background-dominated. These closure tests applied the full background estimation procedure to estimate the backgrounds in the validation regions and compared the estimated background yields to data counts, confirming their agreement.

Finally, these background estimates are used together with signal distributions obtained from MC simulation scaled to HL-LHC cross sections and luminosities to set exclusion limits on production cross sections and upper limits on gluino and top squark masses. Furthermore, projections of 5σ discovery sensitivity were computed.

5 Projection of MC and data event counts

The HL-LHC projections are performed on 2016 simulated and observed events. Simulated events are reweighted to better model data with trigger efficiency corrections, jet energy and resolution smearing, pileup corrections, W and top jet scale factors, b jet tagging scale factors, electron and muon identification and isolation scale factors, and various other corrections specific to the signal event generation and simulation modeling. After these corrections, the object and event selections that define the signal and control regions are applied to these events, as described in Section 4.

To do a projection to the HL-LHC conditions, we first take the M_R-R^2 distributions of the simulated events for each physics process i and each selection region j, and scale the number of events as

$$N^{i,j}_{\text{HL-LHC}} = \left(\frac{\sigma^i_{\text{HL-LHC}}}{\sigma^i_{2016}} \frac{\mathcal{L}_{\text{HL-LHC}}}{\mathcal{L}_{2016}} \right) N^{i,j}_{2016} \tag{4}$$

$$= \kappa^i_{\frac{\text{HL-LHC}}{2016}} N^{i,j}_{2016}, \tag{5}$$

where $N^{i,j}_{2016}$ and $N^{i,j}_{\text{HL-LHC}}$ are the total number of events for a simulated process i in search region j for 2016 and HL-LHC; σ^i_{2016} and $\sigma^i_{\text{HL-LHC}}$ are the cross sections for process i for the 2016 and HL-LHC energies of 13 and 14 TeV; and $\mathcal{L}_{2016}$ and $\mathcal{L}_{\text{HL-LHC}}$ are the 2016 and HL-LHC integrated luminosities of 35.9 fb^{-1} and 3 ab^{-1}.

The scaling applies to both the control and signal regions. Figure 3 shows the $pp \to \widetilde{g}\widetilde{g}$ and $pp \to \widetilde{t}\widetilde{t}$ production cross sections at the next-to-leading-order + next-to-leading-log

(NLO+NLL) level versus the gluino or top squark masses, computed using PROSPINO and NLL-fast [18–22].

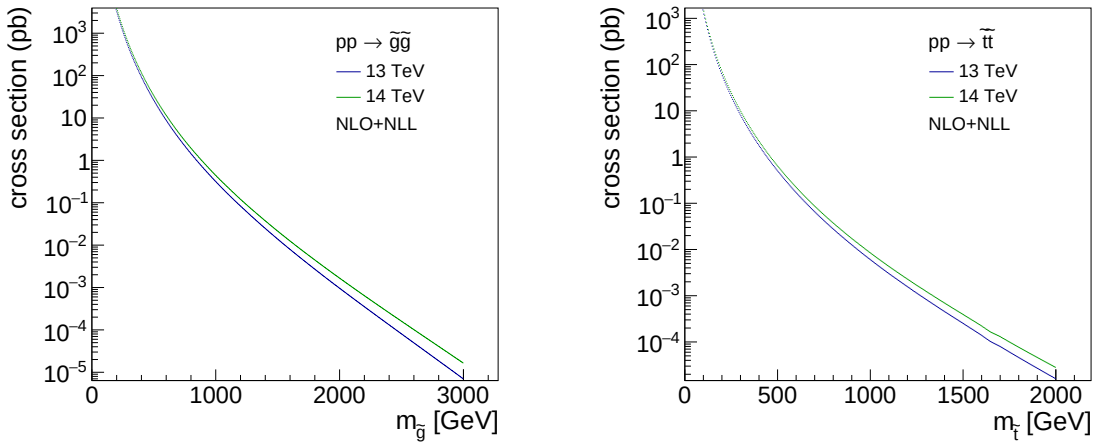

Figure 3: The pp $\rightarrow \widetilde{g}\widetilde{g}$ (left) and pp $\rightarrow \widetilde{t}\widetilde{t}$ (right) production cross sections at NLO+NLL precision versus the gluino and top squark masses, respectively.

Since some background estimates are based on the event yields measured in control regions in data, the correspondent data yields should be scaled to the HL-LHC conditions to deliver the proper projection of the backgrounds. The control regions represent a mixture of some dominant physics processes with minor contributions from additional backgrounds. To properly scale data yields, the simulated events are used. All background processes in MC are scaled to HL-LHC conditions separately and are mixed according to their cross sections to esimate the total event yield in the control region. This yield is compared to the total simulated event yields in the same control region without scaling. The ratio is used to project the existing data-based background estimates to the HL-LHC conditions. We compute this shape-dependent scaling on data distribution $D^{j,k}_{2016}$ in a control region j for each M_R-R^2 bin k as follows:

$$D^{j,k}_{\text{HL-LHC}} = \frac{\sum_i N^{i,j,k}_{\text{HL-LHC}}}{\sum_i N^{i,j,k}_{2016}} D^{j,k}_{2016} \tag{6}$$

$$= r^{j,k}_{\frac{\text{HL-LHC}}{2016}} D^{j,k}_{2016}, \tag{7}$$

where $N^{i,j,k}_{\text{HL-LHC}}$ and $N^{i,j,k}_{2016}$ are yields in bin k of simulated distributions for each process i for a control region j, and the resulting scaling factors $r^{j,k}_{\frac{\text{HL-LHC}}{2016}}$ vary depending on the bin k.

Once the data distributions $D^{j,k}_{\text{HL-LHC}}$ are obtained, a number of pseudo-data events $D^j = \sum_k D^{j,k}$ are produced from the distributions to match the expected yields from the HL-LHC. These pseudo-data event distributions and their statistical uncertainties are used to calculate the estimated backgrounds.

6 Treatment of uncertainties

During the HL-LHC runs, CMS will collect two orders of magnitude more data than it has collected so far in Run 2. This will significantly improve the precision of any analysis result. The large instantaneous luminosity will also cause an increase in the number of pileup events,

which will introduce uncertainties in the results. However, improvements to the detector will help reduce various systematic uncertainties arising from detector inaccuracies and compensate for the pileup effects. The theoretical calculations are also expected to improve, providing more accurate and precise cross sections and event simulations. Furthermore, potential increases in computational speed and storage would help increase the number of simulated events produced and reduce MC-related statistical uncertainties. In this study, we use three scenarios to assess the effects of varying levels of the above-mentioned uncertainties, taken from conventions based on [14]. The integrated luminosities used in defining systematics are $\mathcal{L}_{\text{HL-LHC}} = 3\,\text{ab}^{-1}$ and $\mathcal{L}_{2016} = 35.9\,\text{fb}^{-1}$.

- Run 2 systematic uncertainties: This scenario is useful for direct comparison with the current analyses. Statistical uncertainties are scaled by $1/\sqrt{\mathcal{L}_{\text{HL-LHC}}/\mathcal{L}_{2016}} \equiv 1/\sqrt{\mathcal{L}}$. Systematic uncertainties (including experimental, theoretical and luminosity) are kept the same in relative terms as in the 2016 analysis.
- YR18 (CERN Yellow Report 2018) systematic uncertainties: This scenario reflects uncertainties that are considered achievable from today's perspective for the HL-LHC phase. Statistical uncertainties are scaled by $1/\sqrt{\mathcal{L}}$. Theoretical uncertainties are scaled down by $1/2$. The remaining uncertainties, such as those on luminosity, jet energy scale and resolution, W, top, or b jet tagging scale factors, lepton scale factors, that are considered in the experimental systematic uncertainties category are scaled down based on the recommendations for the Yellow Report. While well-defined percent values were taken for some systematic uncertainties, such as $\pm 1\%$ for luminosity, for others, a fractional or luminosity-based scaling was done, except for the cases where the uncertainties are already small. Table 1 shows the list of uncertainties applied on background and signal processes and the corresponding scaling applied to these with respect to the current analysis.
- Stat-only: This scenario indicates the ultimate precision limit. Statistical uncertainties are scaled by $1/\sqrt{\mathcal{L}}$, while systematic uncertainties are neglected.

The effects of systematic uncertainties applied for the Run 2 and YR18 scenarios vary as a function of M_R and R^2. The uncertainties in the 2016 analysis were dominated by statistical effects. Systematic uncertainties were relatively small for the final states of interest. For the YR18 scenario, some of the Run 2 uncertainties are small, such as those in the lepton reconstruction and identification scale factors, and thus not scaled down. Uncertainties arising from pileup are taken the same as in 2016. Even though pileup is expected to increase by about an order of magnitude, there will be large improvements in tracking, vertexing and η coverage which will compensate for the increased effect. Figure 4 shows the average percentage contributions of the various systematic uncertainties to the overall background estimation as a function of M_R and R^2 bins for the W 4-5 jet, W 6 jet, and Top categories for the Run 2 and YR18 scenarios. The most dominant systematic uncertainties affecting the simulated signal event yields come from W/top tagging ($\sim 8\%$), jet energy scale (JES) ($\sim 3\%$) and b tagging ($\sim 2\%$) variations.

Table 1: Summary of the scaling of uncertainties in the YR18 scenario for the background and signal processes for the HL-LHC projections. The "YR18 recommendation" treatment note specifies that the scaling of the uncertainty was done based on CMS recommendations for the Yellow Report, reflecting the potential upgrade performance of the CMS detector, summarised in Ref. [14].

Uncertainty	Background	Signal	Treatment notes
Statistical uncertainties			
MC event yield	ignored	Run2 $/\sqrt{\mathcal{L}}$	YR18 recommendation
Data event yield	Run2 $/\sqrt{\mathcal{L}}$	–	YR18 recommendation
Extrapolation of background distributions in signal region	ignored	–	YR18 recommendation
Theoretical systematic uncertainties			
Scales (fact., renorm.)	Run2 $\times 1/2$	Run2 $\times 1/2$	YR18 recommendation
α_s	Run2 $\times 1/2$	Run2 $\times 1/2$	YR18 recommendation
Top p_{T} reweighting	Run2 $\times 1/3$	–	YR18 recommendation
ISR reweighting	–	Run2 $\times 1/2$	YR18 recommendation
$Z \to \nu\nu$ modeling	Run2 $\times 1/2$	Run2 $\times 1/2$	YR18 recommendation
Multijet modeling	Run2 $\times 1/2$	Run2 $\times 1/2$	YR18 recommendation
Experimental systematic uncertainties			
Luminosity	$\pm 1.0\%$	$\pm 1.0\%$	YR18 recommendation
Pileup	Run2	Run2	Increased PU but better detector performance
Jet energy/mass scale	Run2 $\times 1/2$	Run2 $\times 1/2$	YR18 recommendation
Jet energy/mass resolution	Run2 $\times 1/2$	Run2 $\times 1/2$	YR18 recommendation
$p_{\mathrm{T}}^{\mathrm{miss}}$	Run2 $\times 1/2$	Run2 $\times 1/2$	from JES, JER
Electron reconstruction	Run2	Run2	small
Electron identification	Run2	Run2	small
Muon tracking	Run2	Run2	small
Muon identification	Run2	Run2	small
Lost lepton shape	Run2 $/\sqrt{\mathcal{L}}$	–	stat-dependent
b tag	$\pm 1\%$	$\pm 1\%$	YR18 recommendation
W/Top tag	Run2	Run2	YR18 recommendation
W/Top mistag	Run2	Run2	YR18 recommendation
W/Top masstag	Run2	–	YR18 recommendation
W/Top antitag	Run2	–	YR18 recommendation
Photon purity	Run2 $\sqrt{\mathcal{L}}$	–	stat-dependent
Direct photon fraction	Run2 $\sqrt{\mathcal{L}}$	–	stat-dependent
Z/γ ratio	ignored	–	small
Z($\nu\bar{\nu}$) closure	Run2 $/\sqrt{\mathcal{L}}$	–	stat-dependent

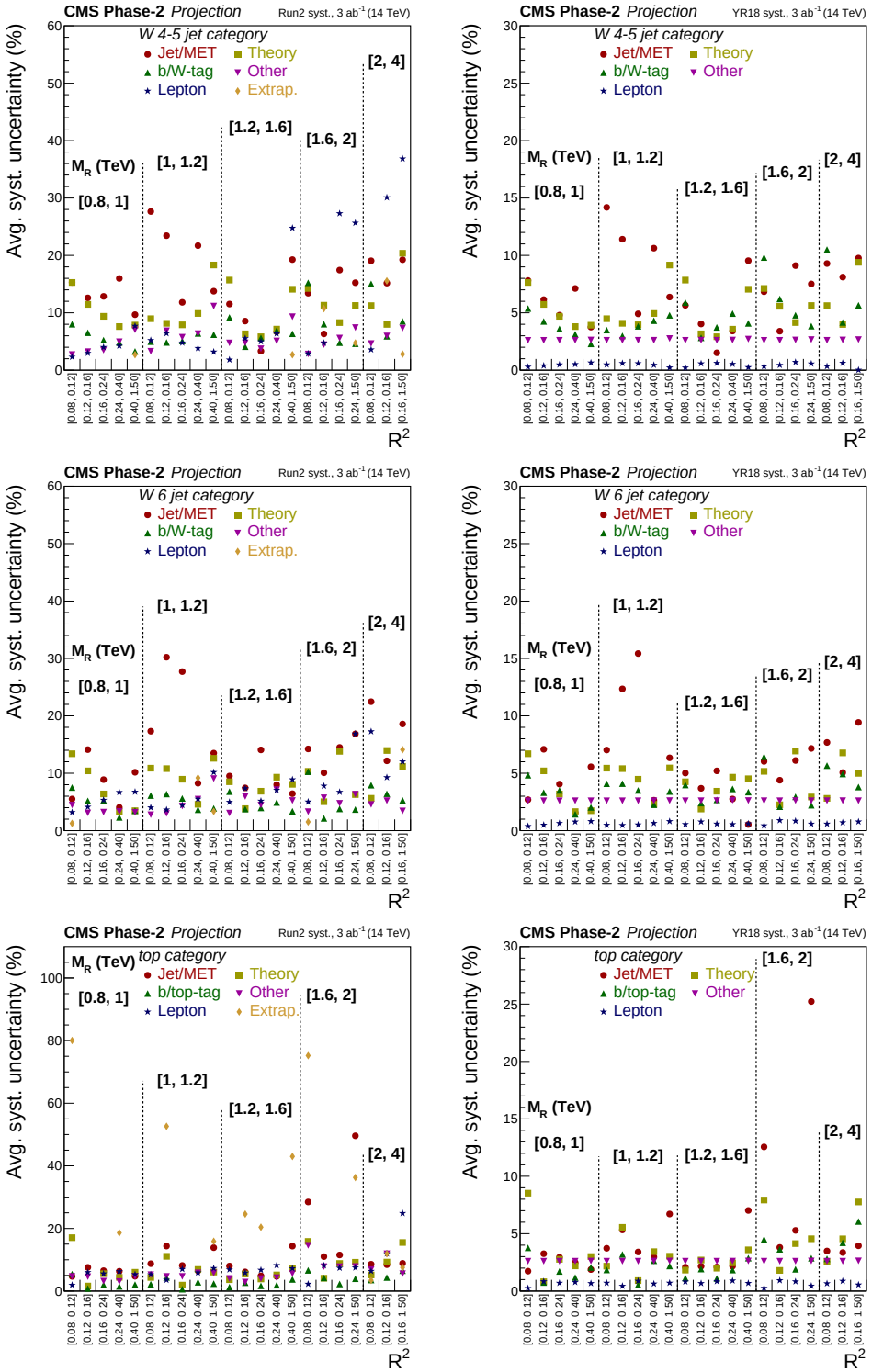

Figure 4: Average percentage contributions of various systematic uncertainties to the overall background estimation under the background-only assumption as a function of bins in M_R and R^2 for the W 4-5 jet (top), W 6 jet (middle), and Top (bottom) categories for the Run 2 (left) and YR18 (right) scenarios.

7 Results and interpretation

We present the overall background estimation for the W 4-5 jet, W 6 jet, and Top categories along with distributions for several signal benchmark scenarios versus a one-dimensional representation of the bins in M_R and R^2 in Fig. 5 for the HL-LHC. Statistical and systematic uncertainties are also shown for the YR18 case where systematic uncertainties are scaled down based on currently estimated projections of luminosity, detector conditions, and theoretical calculations.

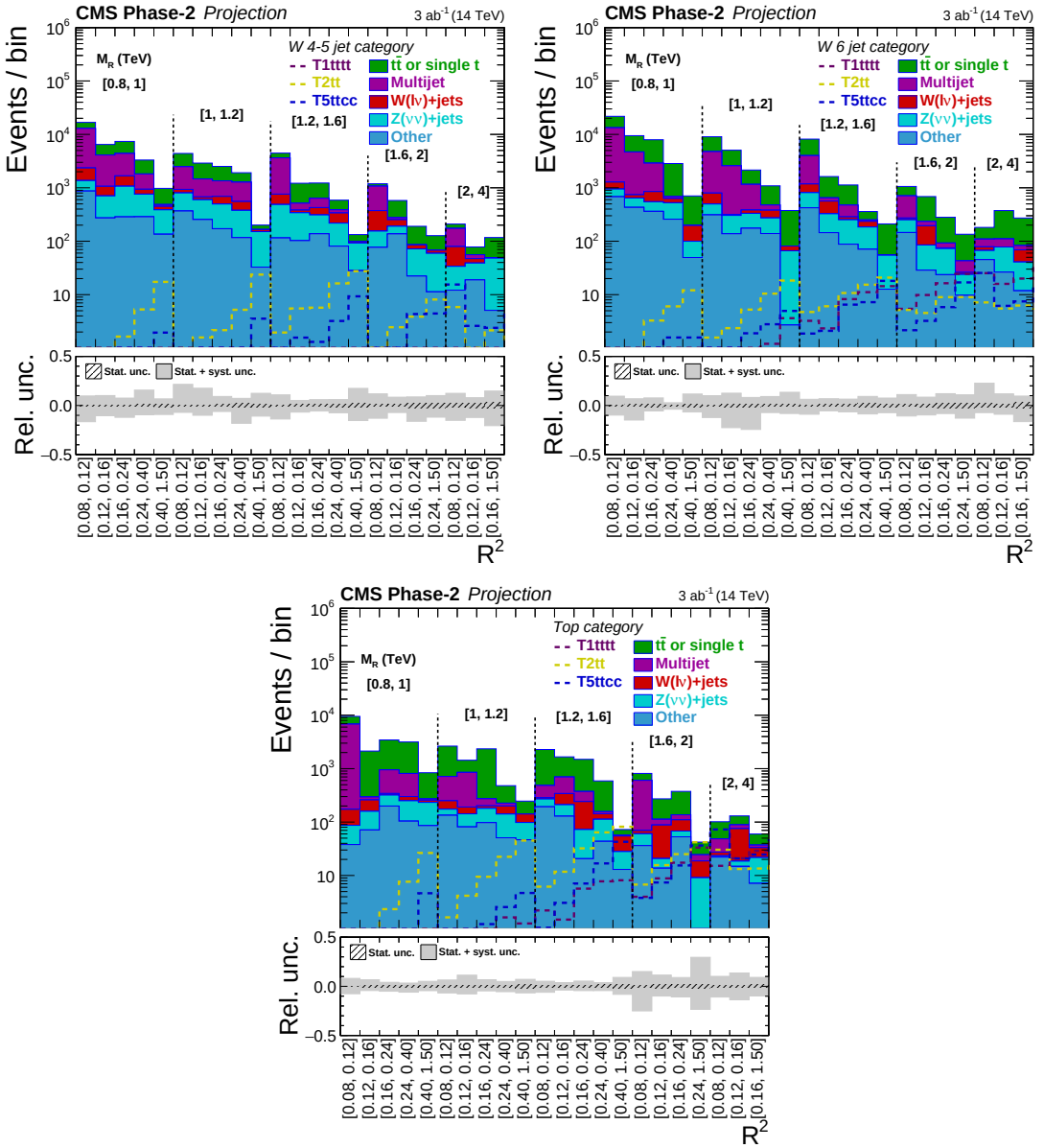

Figure 5: M_R-R^2 distributions shown in a one-dimensional representation for background predictions obtained for the W 4-5 jet (upper left), W 6 jet (upper right), and Top (lower) categories for the HL-LHC. Statistical and systematic uncertainties for the YR18 scenario are shown with the hatched and shaded error bars, respectively. Also shown are the signal benchmark models T5ttcc with $m_{\tilde{g}} = 2\,\text{TeV}$, $m_{\tilde{t}} = 320\,\text{GeV}$ and $m_{\tilde{\chi}_1^0} = 300\,\text{GeV}$; T1tttt with $m_{\tilde{g}} = 2\,\text{TeV}$ and $m_{\tilde{\chi}_1^0} = 300\,\text{GeV}$; and T2tt with $m_{\tilde{t}} = 1.2\,\text{TeV}$ and $m_{\tilde{\chi}_1^0} = 100\,\text{GeV}$.

The results are used to set expected upper limits on the production cross sections of various SUSY simplified models. We follow the LHC CL_s procedure [23–25] by using the profile likelihood ratio test statistic and the asymptotic formula to evaluate the 95% confidence level (CL) expected limits on the production cross section. Systematic uncertainties are propagated by incorporating nuisance parameters that represent different sources of systematic uncertainty, which are profiled in the maximum likelihood fit. Fig. 6 shows the expected upper limits on the signal cross sections for the T5ttcc, T1tttt and T2tt simplified models for the combination of the W 4-5 jet, W 6 jet, and Top categories for the HL-LHC projection based on the YR18 scenario. Additionally, lower limits on gluino/top squark versus neutralino masses are shown for the cases of Run 2 systematic uncertainties, YR18 systematic uncertainties, and statistical-only scenarios. Gluino mass exclusion limit reaches over 2.6 TeV and 2.5 TeV for T5ttcc and T1tttt, respectively, and top squark mass limit reaches over 1.5 TeV for T2tt. For comparison, the figures also show the 2016 mass limits and the 300 fb^{-1} limits for the Run 2 scenario.

Furthermore, projections of expected discovery sensitivity in the presence of a signal are computed. The p-values for the signal plus background and background-only hypotheses are used to obtain the expected significances in terms of number of standard deviations. Figure 7 shows the projected expected significance for the T5ttcc, T1tttt, and T2tt models based on the YR18 systematic uncertainties, along with the discovery upper bounds on the gluino/top squark versus neutralino masses for the three uncertainty scenarios for the HL-LHC. Discovery reach for gluino mass extend over 2.35 TeV and 2.3 TeV gluino mass for T5ttcc and T1tttt, and 1.4 TeV top squark mass for T2tt.

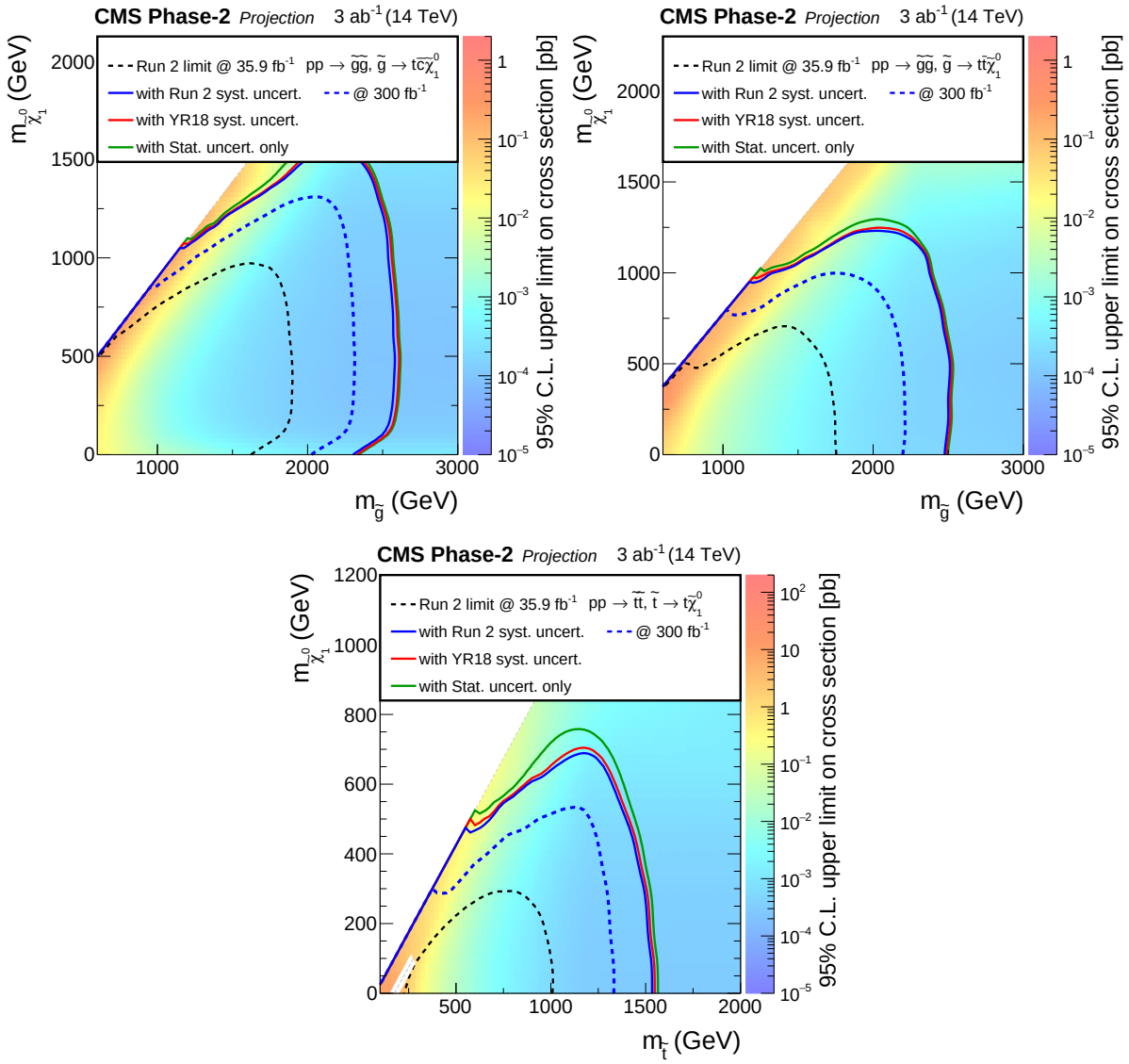

Figure 6: Projected expected upper limits on the signal cross sections for the HL-LHC using the asymptotic CL_s method versus gluino/top squark and neutralino masses for the T5ttcc (top left), T1tttt (top right), and T2tt (bottom) models for the combined W 4-5 jet, W 6 jet, and Top categories for the YR18 scenario. The contours show the expected lower limits on the gluino/stop squark and neutralino masses based on the Run 2 systematic uncertainties, YR18 systematic uncertainties, and statistical-only scenarios, along with the 2016 analysis limit and the $300\,\text{fb}^{-1}$ limit for comparison. The lower left white diagonal band in the T2tt plot corresponds to the region $|m_{\tilde{t}} - m_t - m_{\tilde{\chi}_1^0}| < 25\,\text{GeV}$, where the mass difference between the $\tilde{t}$ and the $\tilde{\chi}_1^0$ is very close to the top quark mass. In this region, the signal acceptance depends strongly on the $\tilde{\chi}_1^0$ mass and is therefore difficult to model.

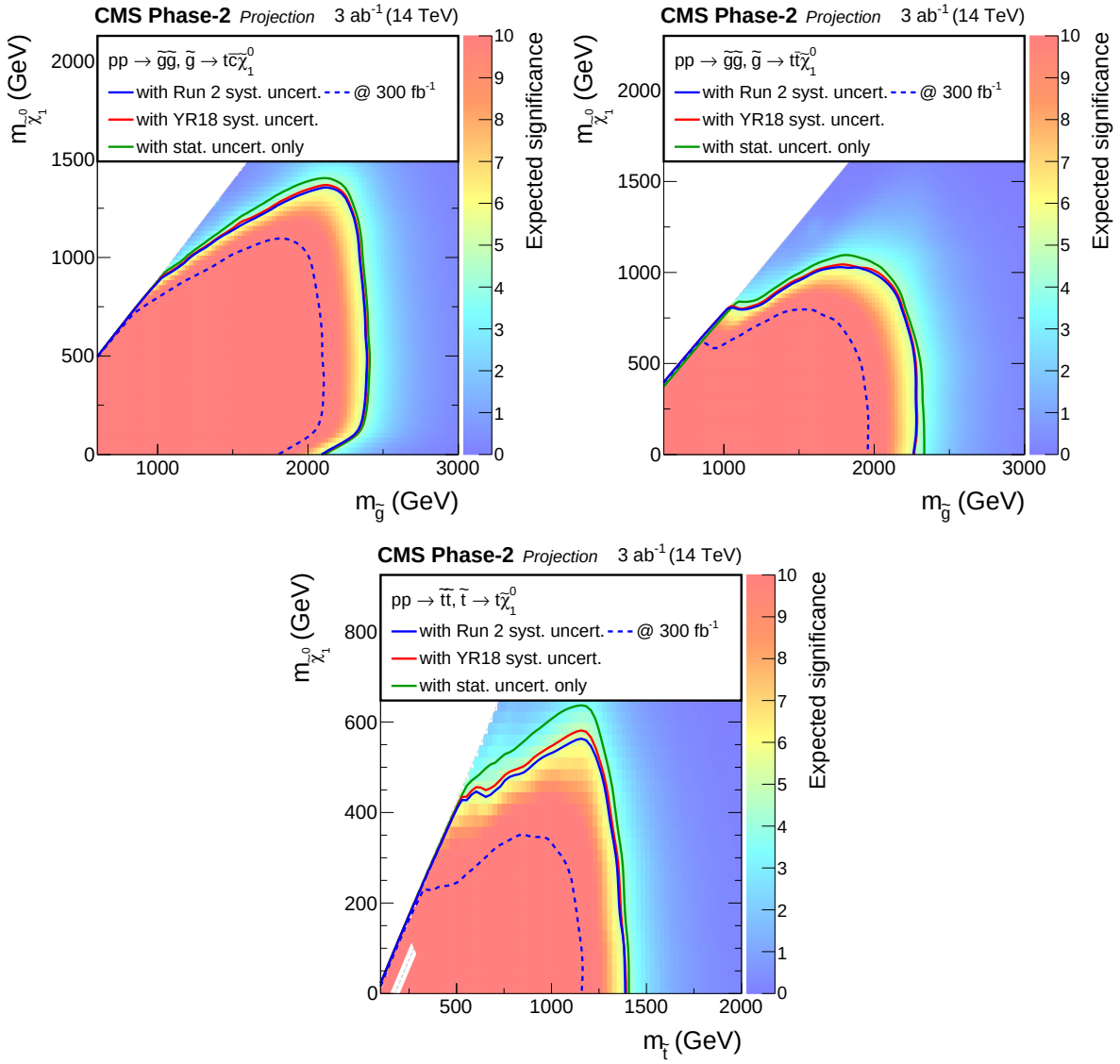

Figure 7: Projected expected significance for the HL-LHC versus gluino/stop and neutralino masses for the T5ttcc (top left), T2tttt (top right), and T2tt (bottom) models for the combined W 4-5 jet, W 6 jet, and Top categories for the YR18 scenario. The contours show the expected discovery bounds on the gluino/top squark and neutralino masses based on the Run 2 systematic uncertainties, YR18 systematic uncertainties, and statistical-only scenarios. The lower left white diagonal band in the T2tt plot corresponds to the region $|m_{\tilde{t}} - m_t - m_{\tilde{\chi}_1^0}| < 25\,\text{GeV}$, where the mass difference between the $\tilde{t}$ and the $\tilde{\chi}_1^0$ is very close to the top quark mass. In this region, the signal acceptance depends strongly on the $\tilde{\chi}_1^0$ mass and is therefore difficult to model.

8 Summary

We have presented the HL-LHC projection of the Run 2 search for new physics in hadronic final states with boosted W bosons or top quarks using the razor kinematic variables. Final states with boosted objects constitute an important search scenario, as they become more accessible at the increased center-of-mass energy at the HL-LHC. The projection study uses observed data yields and simulated signal and background events from the original analysis, which are scaled to obtain the HL-LHC sensitivity for center-of-mass energy of 14 TeV and integrated luminosity of $3\,\text{ab}^{-1}$. The background estimation and limit setting procedures are fully adopted from the Run 2 analysis done using 2016 data. Different scenarios for systematic uncertainties, based on a common convention with other CMS analyses and ATLAS are considered. The projection results are interpreted in terms of gluino pair production where the gluinos decay into either a top quark, an anti-top quark, and a neutralino; or to a top quark and a top squark, and direct top squark pair production where top squarks decay into top quarks and neutralinos. The HL-LHC would exclude gluinos and top squarks up to 2.6 TeV and 1.5 TeV respectively, while making discovery possible for gluinos and top squarks up to masses of 2.35 TeV and 1.4 TeV, respectively, thus providing a very strong test of naturalness scenarios for supersymmetry.

References

[1] CMS Collaboration, "Inclusive search for supersymmetry in pp collisions at $\sqrt{s} = 13$ TeV using razor variables and boosted object identification in zero and one lepton final states", (2018). arXiv:1812.06302. Submitted to *JHEP*.

[2] R. Barbieri and D. Pappadopulo, "S-particles at their naturalness limits", *JHEP* **10** (2009) 061, doi:10.1088/1126-6708/2009/10/061, arXiv:0906.4546.

[3] M. Papucci, J. T. Ruderman, and A. Weiler, "Natural SUSY endures", *JHEP* **09** (2012) 035, doi:10.1007/JHEP09(2012)035, arXiv:1110.6926.

[4] J. Alwall, P. Schuster, and N. Toro, "Simplified models for a first characterization of new physics at the LHC", *Phys. Rev. D* **79** (2009) 075020, doi:10.1103/PhysRevD.79.075020, arXiv:0810.3921.

[5] LHC New Physics Working Group Collaboration, "Simplified models for LHC new physics searches", *J. Phys. G* **39** (2012) 105005, doi:10.1088/0954-3899/39/10/105005, arXiv:1105.2838.

[6] J. Thaler and K. Van Tilburg, "Identifying boosted objects with N-subjettiness", *JHEP* **03** (2011) 015, doi:10.1007/JHEP03(2011)015, arXiv:1011.2268.

[7] C. Rogan, "Kinematical variables towards new dynamics at the LHC", (2010). arXiv:1006.2727.

[8] CMS Collaboration, "The CMS experiment at the CERN LHC", *JINST* **3** (2008) S08004, doi:10.1088/1748-0221/3/08/S08004.

[9] CMS Collaboration, "Technical Proposal for the Phase-II Upgrade of the Compact Muon Solenoid", CMS Technical Proposal CERN-LHCC-2015-010, CMS-TDR-15-02, 2015.

[10] CMS Collaboration, "The Phase-2 Upgrade of the CMS Tracker", CMS Technical Design Report CERN-LHCC-2017-009, CMS-TDR-014, 2017.

[11] CMS Collaboration, "The Phase-2 Upgrade of the CMS Barrel Calorimeter", CMS Technical Design Report CERN-LHCC-2017-011, CMS-TDR-015, 2017.

[12] CMS Collaboration, "The Phase-2 Upgrade of the CMS Endcap Calorimeter", CMS Technical Design Report CERN-LHCC-2017-023, CMS-TDR-019, 2017.

[13] CMS Collaboration, "The Phase-2 Upgrade of the CMS Muon Detectors", CMS Technical Design Report CERN-LHCC-2017-012, CMS-TDR-016, 2017.

[14] CMS Collaboration, "Expected performance of the physics objects with the upgraded CMS detector at the HL-LHC", Technical Report CMS-NOTE-2018-006, CERN-CMS-NOTE-2018-006, 2018.

[15] M. Cacciari, G. P. Salam, and G. Soyez, "FastJet user manual", *Eur. Phys. J. C* **72** (2012) 1896, doi:10.1140/epjc/s10052-012-1896-2, arXiv:1111.6097.

[16] M. Cacciari, G. P. Salam, and G. Soyez, "The anti-k_T jet clustering algorithm", *JHEP* **04** (2008) 063, doi:10.1088/1126-6708/2008/04/063, arXiv:0802.1189.

[17] CMS Collaboration, "Identification of heavy-flavour jets with the CMS detector in pp collisions at 13 TeV", *JINST* **13** (2018) P05011, doi:10.1088/1748-0221/13/05/P05011, arXiv:1712.07158.

[18] W. Beenakker, R. Höpker, M. Spira, and P. M. Zerwas, "Squark and gluino production at hadron colliders", *Nucl. Phys. B* **492** (1997) 51, doi:10.1016/S0550-3213(97)80027-2, arXiv:hep-ph/9610490.

[19] A. Kulesza and L. Motyka, "Threshold resummation for squark-antisquark and gluino-pair production at the LHC", *Phys. Rev. Lett.* **102** (2009) 111802, doi:10.1103/PhysRevLett.102.111802, arXiv:0807.2405.

[20] A. Kulesza and L. Motyka, "Soft gluon resummation for the production of gluino-gluino and squark-antisquark pairs at the LHC", *Phys. Rev. D* **80** (2009) 095004, doi:10.1103/PhysRevD.80.095004, arXiv:0905.4749.

[21] W. Beenakker et al., "Soft-gluon resummation for squark and gluino hadroproduction", *JHEP* **12** (2009) 041, doi:10.1088/1126-6708/2009/12/041, arXiv:0909.4418.

[22] W. Beenakker et al., "Squark and gluino hadroproduction", *Int. J. Mod. Phys. A* **26** (2011) 2637, doi:10.1142/S0217751X11053560, arXiv:1105.1110.

[23] A. L. Read, "Presentation of search results: The CL_s technique", *J. Phys. G* **28** (2002) 2693, doi:10.1088/0954-3899/28/10/313.

[24] T. Junk, "Confidence level computation for combining searches with small statistics", *Nucl. Instrum. Meth. A* **434** (1999) 435, doi:10.1016/S0168-9002(99)00498-2, arXiv:hep-ex/9902006.

[25] ATLAS and CMS Collaborations, "Procedure for the LHC Higgs boson search combination in summer 2011", CMS NOTE/ATL-PHYS-PUB ATL-PHYS-PUB-2011-011, CMS-NOTE-2011-005, CERN, 2011.